

NEW SAR PROCESSOR BASED ON A SUBSPACE DETECTOR

Rémi DURAND⁽¹⁾, Guillaume GINOLHAC⁽²⁾, Philippe FORSTER⁽²⁾, Laetitia THIRION⁽¹⁾

⁽¹⁾ SONDRALab

SUPELEC, 3 rue Joliot Curie, Plateau du Moulon, 91192 Gif sur Yvette - FRANCE

Tel: +(00 33) 1 69 85 18 13

email: remi.durand@supelec.fr

⁽²⁾ GEA - University Paris 10

PST Ville d'Avray, 92410 Ville d'Avray - FRANCE

email: guillaume.ginolhac@u-paris10.fr

ABSTRACT

This paper deals with a new SAR Processor based on a subspace detector used for Man Made Target(MMT) detection. This new algorithm aims at using new models, different from the isotropic point one commonly used in SAR processors. The implementation of Subspace Detector SAR (SDSAR) algorithm is described along the paper and a simple example shows the interest of using models matched to the target.

1. INTRODUCTION

The detection of Man Made Targets embedded in noise, clutter or speckle with a SAR system is a current issue which occupies both the signal processing and the SAR communities. Most techniques used for target detection are postprocessing treatments of SAR images (eg polarimetry...) but very few focus on a preprocessing treatment, operating directly on the received signal. SAR images can be formed with algorithms [1], which are generally based on the isotropic point model. This model assumes that any target can be seen as a single or a set of isotropic points. This assumption is true if the element to image can be considered as a random volume. Scattering properties of an element generally depend on parameters such as its size, orientation and shape. This leads to consider a target as a set of elements, whose scattering properties will be used. If we consider a model suited to MMT, we would certainly be able to improve detection.

For this purpose, we propose to develop a new SAR imaging algorithm by considering an MMT as a set of canonical elements: as an example, an MMT can be seen as a set of plates. To develop such an algorithm, a first idea could be to implement a filter bank matched to different configurations of the chosen model [2] (for example, filters matched to any orientation of plate). This kind of algorithm suffers from several drawbacks. First, many filters are required to cover all existing configurations. Then it would not be robust enough to configurations which have not been foreseen. However, we show in this paper that these problems can be overcome when the set of signals scattered by the chosen model, whatever its configuration (orientation), belongs to a low dimensional subspace. Therefore, we develop an imaging algorithm based on a subspace detector. Each represented pixel of the final image is based on an evaluation of an appropriate Generalized Likelihood Ratio (GLR) [3]. This algorithm has the advantage of taking the scattering properties of the target into account while using a low number of filters.

The paper is organized as follows. We develop in the

first part of the paper a SAR algorithm based on the isotropic point model deduced from detection theory [3]. We call it the Classical SAR (CSAR) algorithm. We show that this algorithm is equivalent to a well known algorithm, the Time Domain Correlation Algorithm (TDCA) [1]. In a second part, we present the new Subspace Detector SAR (SDSAR) algorithm which generalizes the CSAR algorithm to any kind of model. Finally, we consider that a MMT is a set of metallic plates and we particularize the SDSAR algorithm to that case. We compare, as a preliminary study on detection performances, the ability of SDSAR and CSAR algorithms for detection of metallic plates of different orientations and sizes in a white Gaussian noise. In simulations, the SDSAR algorithm shows important improvement in terms of probability of detection compared to CSAR. Moreover interesting robustness properties to plate orientation and size are obtained. The following convention is adopted: italic indicates a scalar quantity, lower case boldface indicates a vector quantity and upper case boldface a matrix. T denotes the transpose operator and H the transpose conjugate.

2. CLASSICAL SAR PROCESSOR (CSAR)

2.1 SAR Data Acquisition

We consider a strip map SAR configuration: an airborne antenna is moving along an axis u . A signal $e(t)$ is emitted towards the scene at every u_i position of the antenna. The distance between two successive positions is δu . The received signal at every u_i position is $z_i(t)$. We make the “stop and go” assumption: the antenna is not moving when emitting and receiving. \mathbf{e} and \mathbf{z}_i denote the sampled signal vectors associated to $e(t)$ and $z_i(t)$.

2.2 The CSAR Detection Problem

Let \mathbf{z} be the concatenation of n vectors \mathbf{z}_i :

$$\mathbf{z} \in \mathbb{C}^M, \quad \mathbf{z} = [\mathbf{z}_1^T \quad \mathbf{z}_2^T \quad \dots \quad \mathbf{z}_n^T]^T \quad (1)$$

For each (x, y) position to image we consider the two hypothesis H_0 and H_1 . The hypothesis H_0 refers to the case where the signal \mathbf{z} , received at every position u_i , is a white Gaussian noise \mathbf{n} , $N(0, \sigma^2 \mathbf{I})$. H_1 refers to the case where \mathbf{z} is the signal scattered by an isotropic point at (x, y) , \mathbf{r} plus a white Gaussian noise \mathbf{n} , $N(0, \sigma^2 \mathbf{I})$. \mathbf{r} is the concatenation of the $\mathbf{e}_{\tau_{x,y,u_i}}$:

$$\mathbf{r} = \left[\mathbf{e}_{\tau_{x,y,u_1}}^T \quad \mathbf{e}_{\tau_{x,y,u_2}}^T \quad \dots \quad \mathbf{e}_{\tau_{x,y,u_n}}^T \right]^T \quad (2)$$

where $e^{\tau_{x,y,u_i}}$ is the emitted signal delayed of τ_{x,y,u_i} . Quantity τ_{x,y,u_i} is the round trip time between the emitter at u_i and the position (x,y) . The detection problem may thus be written:

$$\begin{cases} H_0 : \mathbf{z} = \mathbf{n} \\ H_1 : \mathbf{z} = \alpha \mathbf{r} + \mathbf{n} \end{cases} \quad (3)$$

where α is an unknown complex attenuation coefficient. Let $p(\mathbf{z}|H_1)$ be the probability density function (pdf) of \mathbf{z} for hypothesis H_1 and $p(\mathbf{z}|H_0)$ the pdf of \mathbf{z} for hypothesis H_0 :

$$p(\mathbf{z}|H_1) = \frac{1}{\pi^M \sigma^{2M}} \exp \frac{-(\mathbf{z} - \alpha \mathbf{r})^H (\mathbf{z} - \alpha \mathbf{r})}{\sigma^2} \quad (4)$$

and

$$p(\mathbf{z}|H_0) = \frac{1}{\pi^M \sigma^{2M}} \exp \frac{-\mathbf{z}^H \mathbf{z}}{\sigma^2} \quad (5)$$

2.3 Implementation of the CSAR Detector

To solve the previous problem, we build a Neyman-Pearson detector based on a Generalized Likelihood Ratio Test (GLRT):

$$T_C = \frac{\max_{\alpha \in \mathbb{C}} p(\mathbf{z}|H_1)}{p(\mathbf{z}|H_0)} \underset{H_1}{\overset{H_0}{\leq}} \eta \quad (6)$$

If we consider $\ln T_C$ we have from (4) and (5):

$$\ln T_C = \frac{\|\mathbf{z}\|^2}{\sigma^2} - \min_{\alpha \in \mathbb{C}} \frac{\|\mathbf{z} - \alpha \mathbf{r}\|^2}{\sigma^2} \quad (7)$$

$$= \frac{\|\mathbf{r}^H \mathbf{z}\|^2}{\sigma^2 \|\mathbf{r}\|^2} \quad (8)$$

We choose to build the SAR image by setting the intensity $I(x,y)$ of pixel at (x,y) to:

$$I(x,y) = \ln(T_C) = \frac{\|\mathbf{r}^H \mathbf{z}\|^2}{\sigma^2 \|\mathbf{r}\|^2} \quad (9)$$

Let $I_{TDCA}(x,y)$ be the intensity of the pixel (x,y) given by the Time Domain Correlation Algorithm (TDCA). According to [1] and using (9) we have:

$$I_{TDCA}(x,y) = \|\mathbf{r}^H \mathbf{z}\| = \frac{I(x,y)^{1/2}}{\mu} \quad (10)$$

with $\mu = \frac{1}{\sigma^2 \|\mathbf{r}\|^2}$.

3. SAR PROCESSOR BASED ON A SUBSPACE DETECTOR

As seen in the previous part, the CSAR algorithm considers that a target is a set of isotropic points. As we have seen, none of the scattering properties of the target is taken into account in this model. We propose to develop a SAR processor based on a model which describes MMT in a more realistic way. We choose to build a SAR processor based on a subspace detector. The chosen subspace corresponds to the subspace of the model used to describe the target (as plate, cylinder, dipole or dihedral subspace). We call it the SDSAR (Subspace Detector SAR) algorithm.

3.1 SDSAR Detection Problem

For each position (x,y) to image, we consider two hypotheses H_0 and H_1 . H_0 refers to the case where the received signal, \mathbf{z} , is a white Gaussian noise \mathbf{n} , $N(0, \sigma^2 \mathbf{I})$. H_1 corresponds to the case where the received signal is the signal scattered by the chosen model, with an unknown configuration, plus \mathbf{n} . From now on, we consider that the different configurations of the chosen model correspond to its various possible orientations (θ, ϕ) . The angles (θ, ϕ) are defined in figure 2.

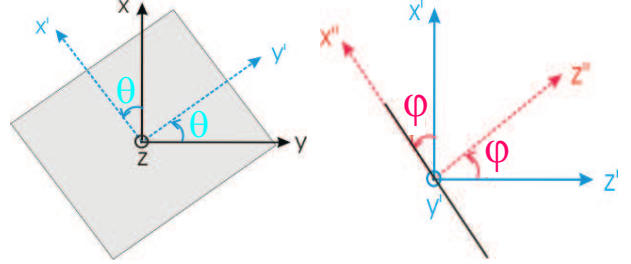


Figure 1: Definition of the orientations θ and ϕ in the case of a plate

The detection problem is written as follows:

$$\begin{cases} H_0 : \mathbf{z} = \mathbf{n} \\ H_1 : \mathbf{z} = \alpha \mathbf{y}(\theta, \phi) + \mathbf{n} \end{cases} \quad (11)$$

where

$$\mathbf{y}(\theta, \phi) = [\mathbf{y}_1(\theta, \phi)^T \quad \mathbf{y}_2(\theta, \phi)^T \quad \dots \quad \mathbf{y}_n(\theta, \phi)^T]^T \quad (12)$$

and $\mathbf{y}_k(\theta, \phi)$ is the signal received at position u_k , scattered by the chosen model at (x,y) with an unknown orientation θ and ϕ . The quantity α is an unknown complex attenuation coefficient. If the set spanned by $\mathbf{y}(\theta, \phi)$ at (x,y) when $(\theta, \phi) \in [0, \pi]^2$, belongs to a subspace $\langle H_{xy} \rangle$ of dimension D , we can rewrite the detection problem as:

$$\begin{cases} H_0 : \mathbf{z} = \mathbf{n} \\ H_1 : \mathbf{z} = \mathbf{H}_{xy} \lambda + \mathbf{n} \end{cases} \quad (13)$$

where \mathbf{H}_{xy} is an orthonormal basis $(M \times D)$ associated to the “subspace model” $\langle H_{xy} \rangle$, and λ is the unknown corresponding $(D \times 1)$ coordinate vector of the signal $\alpha \mathbf{y}(\theta, \phi)$.

3.2 Implementation of the SDSAR algorithm

3.2.1 Implementation of the Subspace Detector

To solve the previous detection problem we use once again the GLRT:

$$T_{SD} = \frac{\max_{\lambda \in \mathbb{C}^D} p(\mathbf{z}|H_1)}{p(\mathbf{z}|H_0)} \underset{H_1}{\overset{H_0}{\leq}} \eta \quad (14)$$

where

$$p(\mathbf{z}|H_1) = \frac{1}{\pi^M \sigma^{2M}} \exp \frac{-(\mathbf{z} - \mathbf{H}_{xy} \lambda)^H (\mathbf{z} - \mathbf{H}_{xy} \lambda)}{\sigma^2} \quad (15)$$

and

$$p(\mathbf{z}|H_0) = \frac{1}{\pi^M \sigma^{2M}} \exp \frac{-\mathbf{z}^H \mathbf{z}}{\sigma^2} \quad (16)$$

If we consider $\ln T_{SD}$, we obtain:

$$\ln T_{SD} = \frac{\|\mathbf{z}\|^2}{\sigma^2} - \frac{\min_{\lambda \in \mathbb{C}^D} \|\mathbf{z} - \mathbf{H}_{xy}\lambda\|^2}{\sigma^2} \quad (17)$$

$$= \frac{\|\mathbf{H}_{xy}^H \mathbf{z}\|^2}{\sigma^2} \quad (18)$$

As previously, we set the intensity of the pixel at position (x, y) , to $I(x, y)$:

$$I(x, y) = \ln T_{SD} = \frac{\|\mathbf{H}_{xy}^H \mathbf{z}\|^2}{\sigma^2} \quad (19)$$

If we compare equation (9) corresponding to CSAR and equation (19) corresponding to SDSAR, we notice that CSAR is a particular case of SDSAR where the basis matrix \mathbf{H}_{xy} is vector $\frac{\mathbf{r}}{\|\mathbf{r}\|}$. This basis describes the 1-dimensional subspace which contains signal scattered by isotropic points. The CSAR algorithm is thus an SDSAR algorithm where the chosen model is the isotropic point model.

3.2.2 Implementation of the Subspace Basis \mathbf{H}_{xy} of $\langle H_{xy} \rangle$

To compute (19), we need to know a basis \mathbf{H}_{xy} of subspace $\langle H_{xy} \rangle$. For a given position (x, y) , $\langle H_{xy} \rangle$ is defined as the subspace which contains the set of the signals scattered by the chosen model at position (x, y) whatever its orientation (θ, ϕ) . Let us consider matrix \mathbf{S}_{xy} defined as:

$$\mathbf{S}_{xy} = [\mathbf{y}(\theta_1, \phi_1) \quad \mathbf{y}(\theta_1, \phi_2) \quad \dots \quad \mathbf{y}(\theta_N, \phi_N)] \quad (20)$$

Each column of \mathbf{S}_{xy} corresponds to the signal $\mathbf{y}(\theta_i, \phi_j)$, scattered by the chosen model at (x, y) with orientation (θ_i, ϕ_j) . (θ_i, ϕ_j) are chosen in $[0, \pi]^2$. We apply a Singular Value Decomposition (SVD) to \mathbf{S}_{xy} :

$$\mathbf{S}_{xy} = \mathbf{U}\Sigma\mathbf{V}^H \quad (21)$$

where \mathbf{U} and \mathbf{V} are two orthonormal matrices and Σ a diagonal matrix containing the singular values of \mathbf{S}_{xy} .

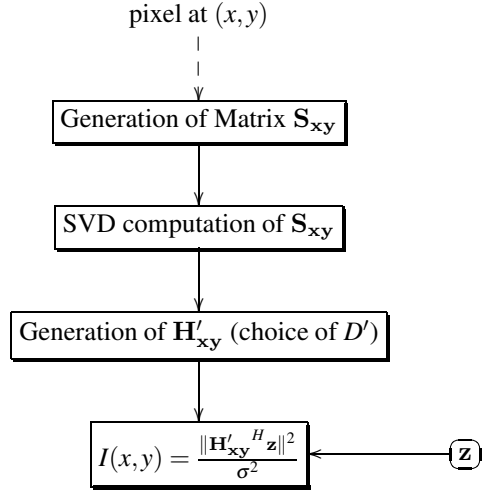
\mathbf{H}_{xy} is given by the D first columns of \mathbf{U} associated to the D first non null singular values. We generally do not use all the D first columns, as a lot of singular values are very small compared to others. To determine the best subspace basis of rank D' ($D' \leq D$), we look for the basis \mathbf{H}'_{xy} which minimizes the following criterion $C(\mathbf{H}'_{xy})$:

$$C(\mathbf{H}'_{xy}) = \sum_{i,j} \|\mathbf{y}(\theta_i, \phi_j)\|^2 - \|\mathbf{H}'_{xy}{}^H \mathbf{y}(\theta_i, \phi_j)\|^2 \quad (22)$$

According to [4], if \mathbf{H}'_{xy} is made of the D' first columns of \mathbf{U} , the criterion $C(\mathbf{H}'_{xy})$ is minimized. The SDSAR algorithm is applied using the basis \mathbf{H}'_{xy} instead of \mathbf{H}_{xy} : its performances will depend on the chosen rank D' .

3.2.3 Implementation of the SDSAR Algorithm

The SDSAR algorithm is summarized in the following scheme:



4. APPLICATION OF THE SDSAR ALGORITHM WITH A METALLIC PLATE MODEL

In this part, we assume that a MMT is a set of metallic plates of different sizes and orientations (as in [5]). We apply the metallic plate model to the SDSAR algorithm: each $\mathbf{y}(\theta_i, \phi_j)$ defined in (12) corresponds to the signal scattered by a plate at a given position (x, y) with orientation (θ_i, ϕ_j) . Our aim in this section is to compare the performances of CSAR and SDSAR algorithms for plates detection. First we define the parameters of the SAR simulation, then we compare the performances of the two algorithms for size-matched and non size-matched plates configurations.

4.1 Simulation parameters

- Code: The code used for $\mathbf{y}(\theta_i, \phi_j)$ computation is based on the physical optics approximation, which requires that plates dimensions are larger than the wavelength. The scattering matrix of a perfectly conducting plate used to compute scattered signals is derived from [6].
- Size: the target model is a $1 m \times 2 m$ metallic plate. The subspace detector is matched to this plate size. The plate subspace generated is a low dimensional one as very few singular values of the signal matrix have a significant intensity (as shown in figure 2).
- Configuration of the scene: A plate is located in the middle of the scene to image, with an orientation (θ, ϕ) .
- Emitted chirp: The central frequency of the chirp is 400 MHz with a bandwidth of 100 MHz.

4.2 SAR imaging and detection of a size matched plate

In this part, the target is a plate which has the same size as the model used to build \mathbf{H}'_{xy} . We first compare the images formed by the two CSAR and SDSAR algorithms, then we compare Detection Probability (DP) versus Signal to white Gaussian Noise Ratio (SNR) for a given False Alarm Probability (FAP).

- Image formation:

As a first example, we consider the configuration described in figure (3.a) where $\theta = 0$ and $\phi = -\pi/4$. Figure 4 represents

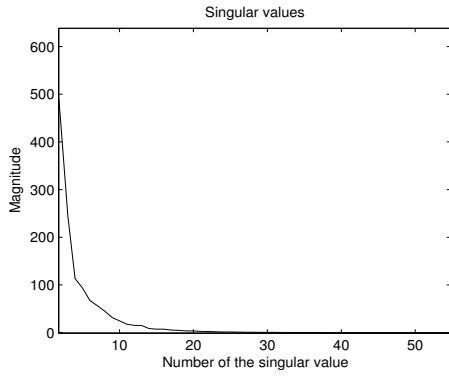


Figure 2: Singular values of a 1×2 m metallic plate signal matrix

the SAR images obtained with CSAR (a) and SDSAR (b, c, d) algorithms. The three SDSAR images correspond to SDSAR of rank 2, 6 and 10 (their corresponding base \mathbf{H}'_{xy} are made with the 2, 6 and 10 first column vectors of \mathbf{U}). The magnitude given by colorbars is $\sigma^2 I(x, y)$. We notice that the spot corresponding to the CSAR case is thinner than the three others, and is located exactly at the phase center of the plate. The spot corresponding to the SDSAR cases becomes larger and larger with the value of the chosen rank. We also observe that the top magnitude from rank 2 to rank 10 is weakly increasing. A high rank subspace (higher than 2) hardly improves the magnitude of the pick corresponding to the plate phase center.

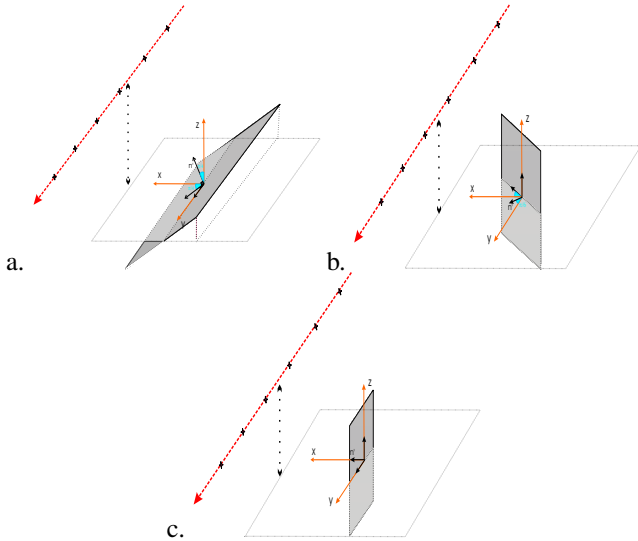


Figure 3: a: plate with orientation $\theta = 0$ and $\phi = -\pi/4$, b: plate m with $\theta = \pi/2$ and $\phi = \pi/6$ and c: plate m with $\theta = 0$ and $\phi = 0$

We consider now the scene described in figure 3.b ($\theta = \pi/2$ and $\phi = \pi/6$). We obtain figure 5 defined as figure 4. The CSAR algorithm image is a spot spread around the plate phase center. SDSAR of rank 2 provides a similar image. The spot is starting to focus on the phase center of the plate for rank 6 and is perfectly focused for rank 10. We also notice

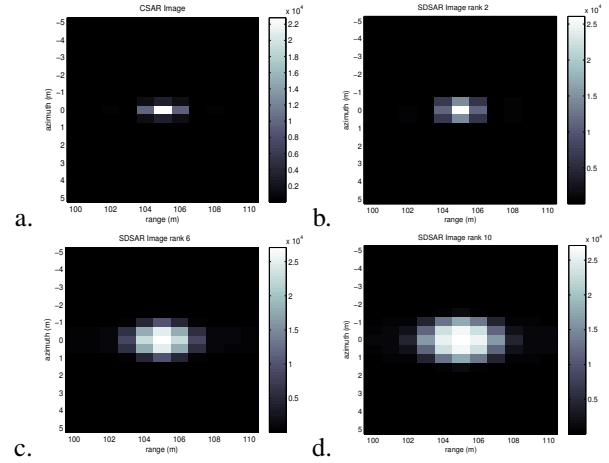


Figure 4: a: CSAR image of a 1×2 m plate with orientation $\theta = 0$ and $\phi = -\pi/4$. b, c, d: SDSAR of rank 2, 6 and 10

that the top magnitude of the image from rank 2 to rank 10 is greatly improving. In this case, using high rank SDSAR algorithms improves the precision of localisation accuracy and significantly increases the magnitude of the pick placed at the center of phase of the plate.

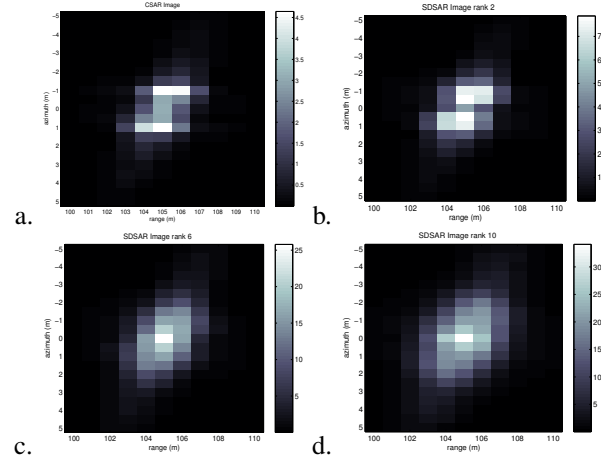


Figure 5: a: CSAR image of a 1×2 m plate with orientation $\theta = \pi/2$ and $\phi = \pi/6$. b, c, d: SDSAR of rank 2, 6 and 10

- Probability of detection versus SNR:

We study in this part the PD versus SNR for a given False Alarm Probability (FAP) of 10^{-5} . FAP corresponds to a χ^2 test statistics with $2D'$ degree of freedom and PD to a non central χ^2 with $2D'$ degree of freedom and with a non central parameter of $\max_{x,y} \frac{\|\mathbf{H}'_{xy} H_y\|^2}{\sigma^2}$. Figures 6 represents CSAR and rank 2, 4, 6, 8 and 10 SDSAR performances for the three configurations given in figure 3. As a reference, we also plot the curve corresponding to the optimal case, when the plate orientation is known. We first notice that for each case, the SDSAR algorithm gives better performances than the CSAR one, from 0 to 5 dB (except in figure 6.a for

SDSAR of rank 8 and 10, where performances are the same than the CSAR, which is a particular case). We also notice that from one case to another, the best performances are not obtained for the same SDSAR rank. The highest PD versus SNR referring to the configuration given in figure 3.a is for rank 2 SDSAR, in figure 3.b, rank 10 and in figure 3.c, rank 4. The first singular vectors in matrix \mathbf{H}'_{xy} are matched to cases where the plate scatters a lot of energy in the synthetic aperture direction (as in figure 3.a). The other vectors, associated to lower singular values, correspond to cases where the plate scatters lower energy in the direction of the synthetic aperture (the worst case here is given in figure 3.b). We can also notice by comparing performances in figure 6a., b. and c. that for SDSAR of rank 8 and 10, performances are nearly the same in the three configurations, whereas lower rank SDSAR performances highly variate. We can conclude that the SDSAR algorithm is robust to orientation for an important enough SDSAR rank (rank 8 and 10).

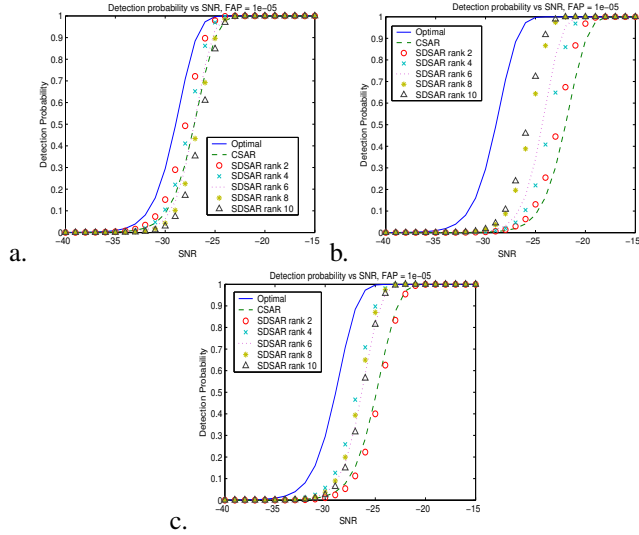


Figure 6: *Detection Probability vs SNR, for $FAP=10^{-5}$, for a 1×2 m plate with orientation a: $\theta = 0$ and $\phi = -\pi/4$, b: $\theta = \pi/2$ and $\phi = \pi/6$ and c: $\theta = 0$ and $\phi = 0$*

4.3 SAR detection of a non-size matched plate

This part deals with the performances of the CSAR and SDSAR algorithms for detecting a metallic plate which size differs from the one chosen for the SDSAR model. We choose a 2×3 m plate as target and we keep a the 1×2 m plate as model. Performances in figure 7 refers to cases given in figure 3.a, b. and c. In these three cases, we can observe an important performance improvements between SDSAR and CSAR algorithms: 2 to 5 dB gain in the first case, 0 to 3 dB in the second one and 0 to 4 dB in the last case. We also notice that in all cases, SDSAR of higher ranks give better performances than lower ones (except for the first case where rank 4 and 6 are a little better). If we compare these results to the previous paragraph, where the plate used as target was “size matched”, same performances are once again noticed for SDSAR of high ranks (8 and 10). We can conclude that the SDSAR algorithm is robust to significant plate size variations for a high enough rank SDSAR.

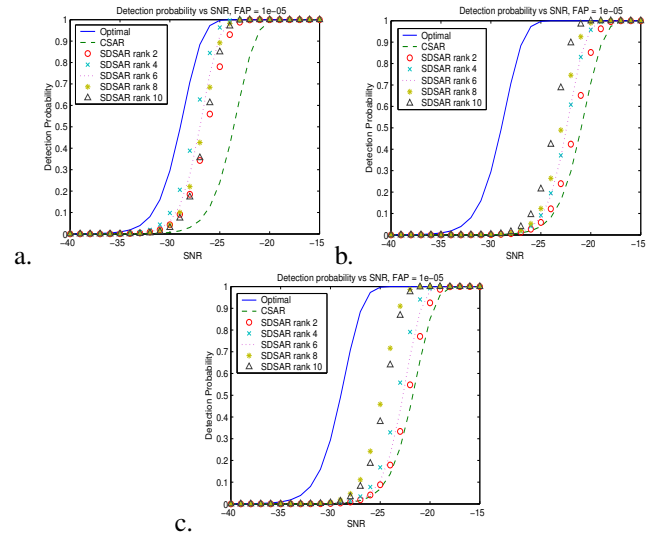


Figure 7: *Detection Probability vs SNR, for $FAP=10^{-5}$, for a 2×3 m plate with orientation a: $\theta = 0$ and $\phi = -\pi/4$, b: $\theta = \pi/2$ and $\phi = \pi/6$ and c: $\theta = 0$ and $\phi = 0$*

5. CONCLUSION

We described in the paper the SDSAR algorithm, a new SAR processor based on a subspace detector. It aims at using other models than the isotropic one. These new models give a suitable description of Man Made Targets that increase detection. For plates detection applications, we noticed that, when using a plate as model, the SDSAR algorithm significantly improves detection performances compare to the CSAR one. The SDSAR algorithm shows robustness properties to plate orientation and size variations. These interesting properties make us optimistic for future applications on more complex “plate made” targets.

REFERENCES

- [1] M. Soumeckh, *Synthetic Aperture Radar Signal Processing*. John Wiley & Sons, inc.
- [2] M.Allen, J.M.Jauregui, L.E.Hoff, “FOPEN-SAR Detection by Direct Use of Simple Scattering Physics” in *IEEE International Radar Conference*, 1995.
- [3] L.L.Scharf, *Statistical Signal Processing: Detection, Estimation and Time Series Analysis*. Addison-Wesley Publishing Co., 1990.
- [4] P.Forster, “Generalized Cross Spectral Matrices for Array of Arbitrary Geometry”, *IEEE transaction on Signal Processing*, vol. 49, n^o5, May 2001.
- [5] M. Dehmollaian, K. Sarabandi, “A Forward Scattering Model for Foliage Camouflaged Complex Target,” in *IGARSS 04, Proceedings 2004, IEEE International*, vol 1, pp258-261, 20-24 Sept 2004.
- [6] F.T.Ulaby, C.Elachi. *Radar Polarimetry for Geoscience Applications*. F.T.Ulaby, C.Elachi Editors.